



# Direct Growth of Vertically-oriented Graphene for Field-Effect Transistor Biosensor

Shun Mao<sup>1</sup>, Kehan Yu<sup>1</sup>, Jingbo Chang<sup>1</sup>, Douglas A. Steeber<sup>2</sup>, Leonidas E. Ocola<sup>3</sup> & Junhong Chen<sup>1</sup>

<sup>1</sup>Department of Mechanical Engineering, University of Wisconsin-Milwaukee, 3200 North Cramer Street, Milwaukee, WI 53211, USA, <sup>2</sup>Department of Biological Sciences, University of Wisconsin-Milwaukee, 3209 North Maryland Avenue, Milwaukee, WI 53211, USA, <sup>3</sup>Center for Nanoscale Materials, Argonne National Laboratory, 9700 South Cass Avenue, Argonne, IL 60439, USA.

SUBJECT AREAS:  
ELECTRONIC PROPERTIES  
AND DEVICES  
NANOSENSORS  
BIOSENSORS  
NANOSTRUCTURES

Received  
17 December 2012

Accepted  
5 April 2013

Published  
22 April 2013

Correspondence and  
requests for materials  
should be addressed to  
J.H.C. (jhchen@uwm.  
edu)

A sensitive and selective field-effect transistor (FET) biosensor is demonstrated using vertically-oriented graphene (VG) sheets labeled with gold nanoparticle (NP)-antibody conjugates. VG sheets are directly grown on the sensor electrode using a plasma-enhanced chemical vapor deposition (PECVD) method and function as the sensing channel. The protein detection is accomplished through measuring changes in the electrical signal from the FET sensor upon the antibody-antigen binding. The novel biosensor with unique graphene morphology shows high sensitivity (down to  $\sim 2$  ng/ml or 13 pM) and selectivity towards specific proteins. The PECVD growth of VG presents a one-step and reliable approach to prepare graphene-based electronic biosensors.

Graphene, a two-dimensional hexagonal network of carbon atoms, has been extensively investigated since 2004 for various applications due to its prominent structural and electrical properties<sup>1–4</sup>. Recent studies have shown that graphene has high sensitivity to electrical perturbations due to its ultra-small thickness and high carrier mobility at room temperature<sup>5</sup>; combining its unique transport properties and structure, graphene is attractive for a variety of sensing applications, e.g., biosensors<sup>6–13</sup>, water sensors<sup>14,15</sup>, and gas sensors<sup>16–19</sup>. A number of studies reported the use of graphene in biosensors, and electrical detection of biomolecules using ultrathin 2D graphene sheets can potentially achieve high sensitivity. This is because graphene is extremely sensitive to electronic perturbations and its surrounding environment, and also because graphene has a large specific surface area, which enables surface functionalization with probe proteins/DNAs<sup>10,20–24</sup>. Although graphene-based biosensors present excellent performance in biomolecular detection, the sensor performance should be further improved to meet demanding requirements in terms of sensitivity, selectivity, and stability; the sensor fabrication method also should be suitable for large-scale manufacturing critical for future product/technology commercialization.

Vertically-oriented graphene (VG), also referred to as “carbon nanowall” (CNW), is a two-dimensional “graphitic” platelet that is typically oriented vertically on a substrate<sup>25–29</sup>. The unique vertical orientation and open structure make VG an ideal sensing material as its entire surface is accessible by analyte molecules. Recently, our group has developed a dc plasma-enhanced chemical vapor deposition (dc-PECVD) approach for atmospheric pressure growth of vertical graphene on various conductive substrates<sup>30–32</sup>. This approach can serve as a simple and one-step method to prepare graphene-based field-effect transistor (FET) devices and can be a better alternative route to drop-casting methods that are commonly used to fabricate graphene and carbon nanotube (CNT) FET devices. Because the vertically-oriented graphene is directly grown on the sensor electrode, it is believed that this platform could achieve higher stability and repeatability than the drop-casting method, which in general has a high noise level and poor stability due to the weak binding between the graphene sheet and the sensor electrode.

In this study, a graphene FET biosensor is fabricated through direct growth of vertical graphene sheets on the sensor electrode through PECVD and subsequent deposition of Au NP-antibody conjugates on the VG surface. The binding of probe and target proteins will induce a significant change in the electrical conductivity of the FET sensor and can be sensitively measured in FET and direct-current tests. The new protein sensors show high sensitivity (down to  $\sim 2$  ng/ml or 13 pM) and selectivity to specific proteins and are especially attractive for large-scale fabrication of sensor devices since the graphene growth and the assembly are accomplished in one step. The sensitivity of the VG sensor is also among the best of carbon nanomaterial (e.g., CNT and graphene)-based protein sensors, which have a detection limit typically from fM to nM<sup>11,21,33–36</sup>. Previous studies have shown that the FET sensor signal is largely dependent on the initial sensor resistance and varies from sensor to sensor<sup>37</sup>. With



the PECVD method, multiple sensors can be fabricated in the same experiment under the same growth conditions; therefore, it is possible to control the initial resistance level of the sensor device and minimize variations in the sensor signal. Moreover, by designing the substrate (sensor electrode) patterns, VG could grow along the patterns and create various sensor structures for different applications. The new VG-based sensing platform could serve as a general platform for biomolecular detection because of its easy fabrication and controllable sensor structure.

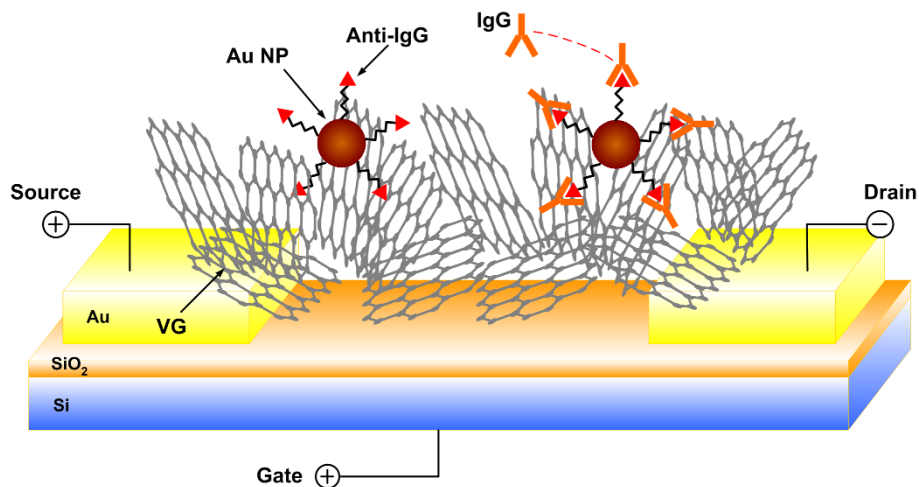
## Results

Figure 1 shows a schematic of the VG FET sensor through direct growth of VG between the drain and the source electrodes. The FET sensor is constructed with VG sheets as the sensing channel, whose conductivity change is measured as the sensing signal through transistor and direct-current measurements. This sensor configuration allows for the direct diffusion and binding of the target protein (antigen in the solution) to the probe protein (antibody functionalized on the Au NP). To investigate the sensor structure and the VG alignment on the gold electrode, scanning electron microscope (SEM) images of the sensor electrode after the growth of VGs are shown in Fig. 2. The sensor electrode is a two parallel fingers design and after the PECVD growth, due to the electric field distribution, VGs are found grown mainly along the two parallel fingers area (Fig. 2a). Based on larger magnification SEM images (Fig. 2b and c), VGs are vertically grown on the gold electrode and extend into a three-dimensional network. With a large specific surface area and a vertical structure, Au NP-antibody conjugates are easily deposited and attached to the VG surface, as shown in the SEM images. The nanoparticle distribution on the VG surface is uniform and no agglomeration is observed. To further investigate the number of layers in the VG sheets and also the sheet network structure, transmission electron microscope (TEM) and high-resolution TEM (HRTEM) images of the VG are shown in Fig. 2d and 2e. The VG sheets show a crumpled structure and are grown and accumulated from the bottom of the electrode; on the top area of the VG, single pieces of graphene sheets are found. HRTEM images indicate that the VG sheet has 4–6 layers, which is in accordance with previously reported VG structures<sup>32</sup>. Since the VG structure is similar to that of multilayer graphene, it is expected that VG will have similar electrical properties. Fig. 2f and 2g show TEM and HRTEM images of the VG network with Au NP-antibody conjugates. The images clearly show that Au NPs are uniformly distributed on the VG surface and the HRTEM image confirms that the Au NPs have a good crystalline structure with a lattice spacing of 0.236 nm, which matches well with

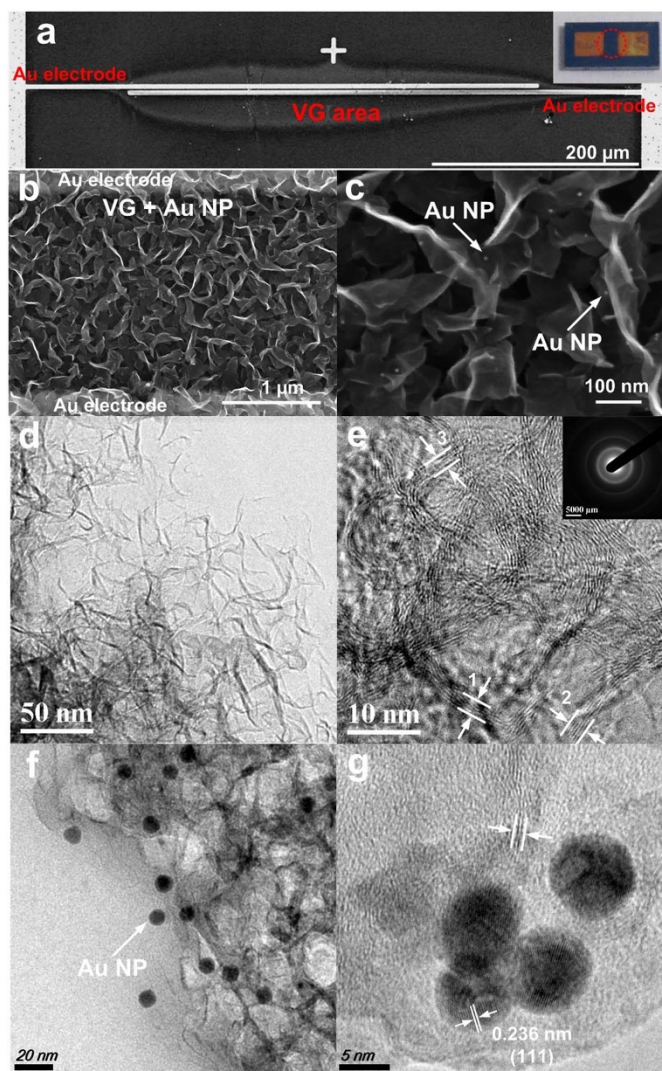
the lattice spacing of Au (111). On the basis of the HRTEM image, the size of Au NPs is confirmed as  $10 \pm 2$  nm. Energy-dispersive X-ray spectroscopy (EDX) profile is also obtained for hybrid VG-Au NP structures as shown in the Supplementary Information (Fig. S1).

Figure 3a shows the direct current measurement results of the sensor after fabrication and under biochemical treatments. The resistance level of the VG devices ranges in  $10^3$ – $10^4$   $\Omega$  under the current growth condition; after the deposition of Au NP, blocking buffer (BB) incubation, and Immunoglobulin G (IgG) injection, the sensor resistance keeps increasing. Since the VG showed a semiconducting behavior in an ambient environment<sup>38</sup>, FET measurements were carried out to further explore the sensor response to target biomolecules. The p-type nature of the VG in an ambient condition was confirmed by the FET transport characteristics (Fig. 3a, inset). In the sensing step (Fig. 3b), with the introduction of the IgG solution to the sensor, the drain current  $I_d$  decreased. Therefore, the FET measurement results indicate that the sensor resistance increases after the addition of IgG, which is also in agreement with the I–V measurement results. The slopes of FET curves were almost identical before and after the introduction of IgGs (slight change in on-off ratio from 1.11 to 1.09), indicating that the attached IgGs have an insignificant effect on the carrier mobility in the VG. Therefore, a change in the carrier density due to the electric field gating effect might be responsible for the resistance change in the VG<sup>37</sup>. A detailed discussion on the conductivity change in the VG sensor is included in the Supplementary Information. To quantitatively evaluate the sensor response, the sensor sensitivity is defined as  $\Delta R/R_0$ , in which  $\Delta R$  is the sensor resistance increase and  $R_0$  is the sensor original resistance before IgG injection. Over ten VG sensors were prepared and tested for IgG with the same concentration (2 ng/ml), and the sensor sensitivity was in the range of 4.5–15%.

For a nanostructure-based electronic sensor, the modification to the nanomaterial conducting channel (VG) is critical to the function of the sensor. To better understand the function of Au NP-antibody conjugates and the BB, control experiments were performed on a VG device, i.e., a device without Au NP anti-IgG functionalization or without the BB incubation. The sensing results of a device without Au NP anti-IgG functionalization are shown in Fig. 3c, in which the device resistance increased with the IgG (2 ng/ml); however, the sensor sensitivity (0.4–4.8%) was much smaller than that with the probe proteins. This result indicates that the surface functionalization of VG (conducting channel) with probe proteins is critical for the function of the sensor and poor functionalization with the probe protein will lead to sensor failure. In another control experiment, the function of BB was studied. Based on results from controlled experi-



**Figure 1** | Schematic of the VG FET sensor by direct growth of VG between the drain and the source electrodes. Probe antibody is labeled to the VG surface through Au NPs.



**Figure 2 | Sensor structure characterization with SEM and TEM.** (a) SEM image of one pair parallel finger electrodes on a silicon wafer, VG is grown in the finger area; inset is the digital image of the sensor electrode. (b) SEM image of VG network between electrode fingers after deposition with Au NP-antibody conjugates. (c) magnified SEM image of VG network deposited with Au NP-antibody conjugates. (d) and (e) TEM and HRTEM images of VG network; the inset shows the SAD pattern of the VG; locations 1, 2, and 3 show VG sheets with 5, 6, and 4 layers, respectively. (f) and (g) TEM and HRTEM images of VG network with Au NP-antibody conjugates.

ments (Fig. 3d), the sensor showed a much higher response (150%) to the same concentration of IgG than sensors treated with BB. Therefore, the sensor response is coming from the non-specific binding of IgGs to the VG and possibly the electrode, which leads to the change in the VG conductivity.

For an electronic sensor, the response time of the sensor is also an important factor for determining its widespread use. Therefore, to study the dynamic response of the sensor, target proteins with different concentrations were manually injected onto the sensor surface and the sensor response ( $I_d$ ) was recorded with a constant bias across the electrode. Fig. 4a and b show the dynamic responses of VG sensors with and without probe proteins, respectively. At the beginning of the test, a PBS buffer was injected onto the sensor surface to create an aqueous environment on the VG area, which resulted in a huge decrease in the sensor conductivity. The change in the sensor conductivity is believed to be coming from the change of the VG testing environment from air to aqueous. However, after the injection

of the PBS buffer, the sensor conductivity was stable and suitable for subsequent sensing tests. With the injection of the IgG, the sensor conductivity decreased correspondingly and the sensor response time was short (several seconds). Ideally, the sensor response level is proportional to the target protein concentration; however, for our sensor, the response of the sensor to 2 ng/ml IgG (3.4%) was larger than that of 20 ng/ml IgG (1.5%). This phenomenon is possibly because the number of protein binding sites on the VG (on Au NP) is limited and partially saturated after the first injection of IgG; therefore, the following injection of higher concentration IgG leads to a smaller sensor response than expected. For comparison, a sensor without probe protein immobilization was prepared and tested; the results show that the sensor without probe proteins has a much smaller response (1.2%) to 2 ng/ml IgG and almost no response to a following injection of 20 ng/ml IgG. This finding is in accordance with the previous FET results and further confirms that probe proteins are critical for the successful function of the VG sensors.

The specificity/selectivity of a biosensor is another important parameter for sensor function. To verify the specificity of the sensor, Immunoglobulin M (IgM, 0.2 mg/mL) and horseradish peroxidase (HRP, 0.2 mg/mL) were used as mismatched proteins and introduced to the sensor with exactly the same procedure as that used for the IgG. Sensitivities of the sensors are summarized in Fig. 4c for IgG, IgM, and HRP with and without anti-IgG probes. The sensor responses from the mismatched IgM (3.0%) and HRP (2.4%) are significantly smaller than those from the complementary IgG (9.8%). Sensors with no probe protein immobilization generally showed lower sensitivity to those with the probe proteins.

## Discussion

For our VG sensor, the growth of the VG was regulated by the electric field distribution above the growth substrate, which in our case was the gold electrode. The electric field near the edges of the gold electrodes was much larger than that above the SiO<sub>2</sub>, and the carbon source gas was ionized more efficiently above the gold electrode, so that VG growth started from the edge of the gold electrodes. Since VGs cannot be grown on the SiO<sub>2</sub> surface, VGs themselves could play a role as growth sites. It was assumed that VGs could be grown on the pre-grown VGs due to the relatively higher electric field above these VGs. Therefore, the VG growth started from the edge of the gold electrode and migrated to spacings between the electrode fingers and finally linked the electrode. By taking advantage of the field-selectivity and the expanding growth of VGs, three-terminal FET sensors were fabricated using the resulting VG as the conducting channel. In our previous study<sup>32</sup>, by designing substrate patterns, e.g., a network of squares or the letters U, W, and M, VGs were grown on those grounded squares or letters. Therefore, it is possible to fabricate VG sensors with various shapes by designing electrode patterns.

The resistance measurement results indicate that the VG conductivity level is similar to that of graphene. In our VG sensor, we attribute the sensor resistance change to the VG channel rather than the electrode-VG contact due to a couple of reasons. First, the binding between the VG and gold electrode is pretty strong because VG is directly grown on the gold electrode under a high temperature (700°C in PECVD growth) and the gold electrode surface is partially melted and merged with the VG during the VG growth process. So the contact resistance between the VG and the electrode is very small, which is evidenced by the linear I-V curve shown in Fig. 3a. Second, the VG is a vertical structure and there are very few Au NPs around the VG-electrode contact area. In addition, the BB covers the contact area in the sensing test. Therefore, it is believed that there are limited proteins attached in the contact area during the sensing and the change in the sensor conductance is mainly from the VG channel. Transistor measurements from the sensor show that the VG is a p-type semiconductor with a low  $I_d$  under a positive gate potential. A relatively small (around 1.1) transistor on-off ratio can be extracted

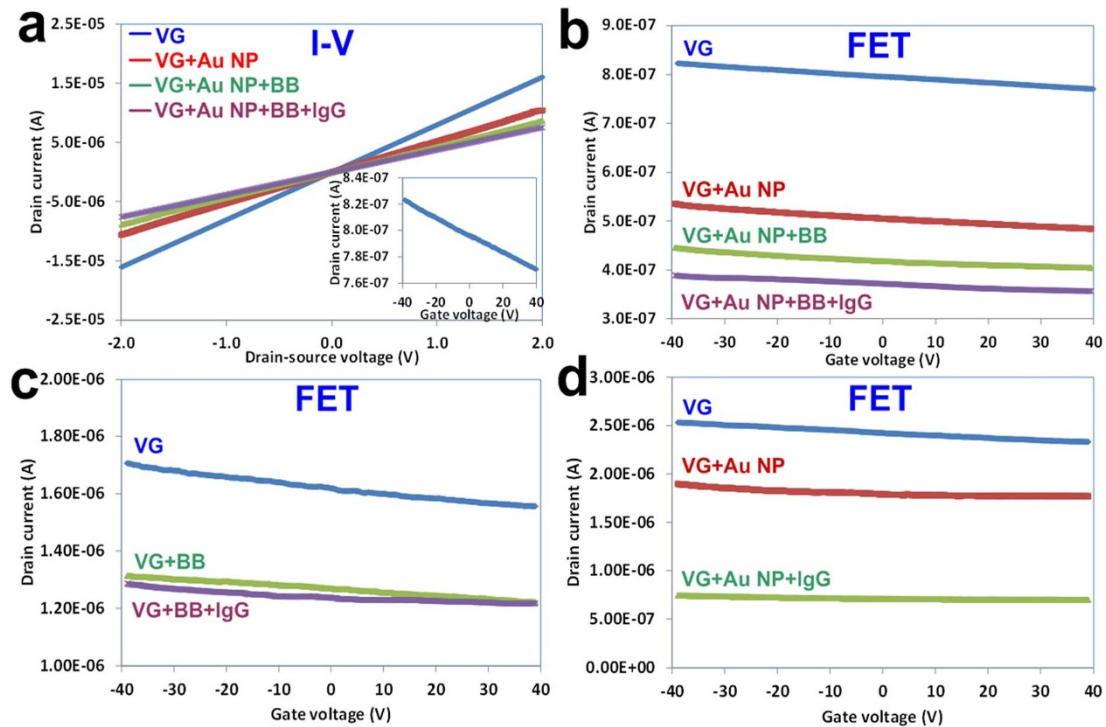


**Figure 3 | Sensor sensing tests with I-V and FET measurements.** (a) Direct current measurement results of the VG sensor modified with Au NP-anti-IgG conjugates, BB, and IgG. Inset is the typical FET curve of the VG sensor. (b) Transistor measurement results of the VG sensor modified with Au NP-anti-IgG conjugates, BB, and IgG (2 ng/mL). (c) Transistor measurement results of the control VG sensor without Au NP-anti-IgG conjugates. (d) Transistor measurement results of the control VG sensor without the BB. For FET measurements,  $V_d = 0.1$  V unless otherwise specified.

from the FET curve. It is believed that the on-off ratio is related to the number of VG sheets between the gold electrode gap. In our previous work<sup>32</sup>, the on-off ratio of the VG FET could be as high as 2.0 and the p-type semiconducting nature of the VG in ambient condition was confirmed from opposite conductivity changes of VG in reducing ( $\text{NH}_3$ ) and oxidizing ( $\text{NO}_2$ ) gases. The sensor sensitivity is one order of magnitude lower than previously reported RGO sensors<sup>10,37</sup>, mainly due to the VG's multiple-layer structure; in general, fewer-layer graphene sensors have higher sensor sensitivity. One possible route to improve the sensor sensitivity is to decrease the number of graphene layers in the VG, which could be realized by controlling the

VG growth conditions (e.g., carbon gas source or gas concentration). For PECVD-grown VG, oxygen groups ( $-\text{COOH}$  and  $-\text{COH}$ ) are present in the graphene layers<sup>39</sup> and may also influence the sensor sensitivity as the VG FET on-off ratio and carrier density are related to the amount of oxygen groups in the graphene carbon lattice.

In commonly used bimolecular detection platforms, e.g., Enzyme-linked immunosorbent assay (ELISA) and Western Blotting, a blocking buffer is needed to eliminate the non-specific binding of the target proteins and can thus lower the uncertainty of detection. Based on this study and on previous experiments, we note that treating the device with BB can effectively diminish the undesirable

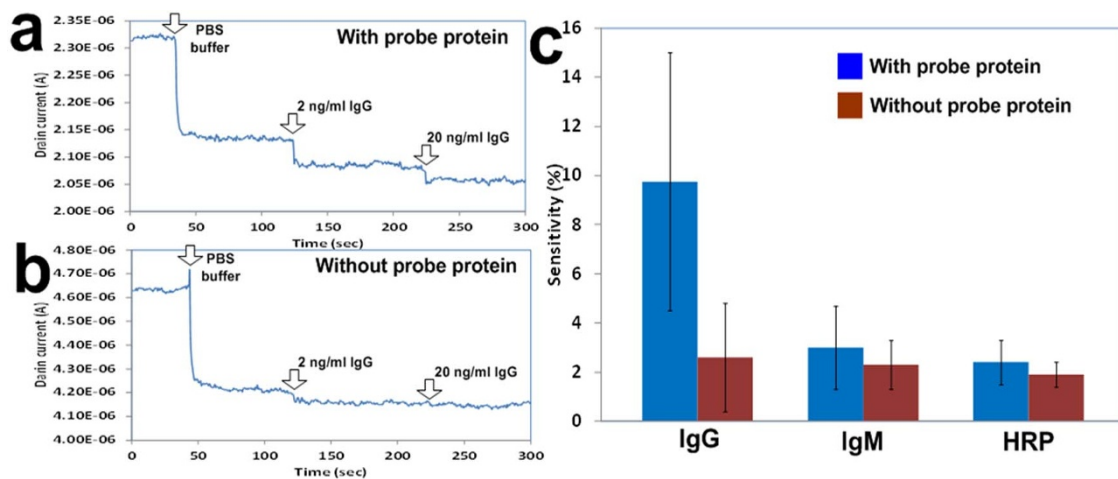


**Figure 4 | Sensor dynamic tests and specificity data.** Dynamic response of the VG sensor exposed to different concentrations of IgG (a) with and (b) without probe proteins. For all measurements, the drain-source voltage  $V_d$  was fixed at 0.01 or 0.1 V. (c) Comparison of the sensor sensitivity in response to complementary IgG (2 ng/mL), mismatched IgM (0.2 mg/mL), and mismatched HRP (0.2 mg/mL). Error bars were obtained from five samples tested for each analyte.



response from the non-specific binding of analytes to the device and is necessary for the specific function of the sensor. One interesting phenomenon is that, with probes, the sensor sensitivities to mismatched proteins are a little bit larger than those without probes, indicating that some non-specific binding between probes and mismatched proteins may occur due to similarities in the protein structures. The specificity result further confirms that the sensor response is from the binding of IgGs to anti-IgGs and the VG sensor has good selectivity to specific proteins.

By comparing the VG sensor with other graphene/reduced graphene oxide-based electronic sensors, this type of sensor shows several advantages. First, the fabrication of the graphene sensor is completed in one single step, and the sensor is ready to use after the CVD growth and no washing or thermal annealing is needed, greatly decreasing the burden of preparing sensor devices. Second, because the graphene sheets are directly grown on the gold electrode, the binding between the graphene and the electrode is strong. The sensor can easily sustain its vertical structure after several incubation and washing treatments, a common issue/drawback for graphene sensors prepared by the drop-cast/film transfer method. Moreover, the vertical hollow graphene structure facilitates bimolecular migration in the buffer solution and thus it is possible to design a sensor with a fast response. This type of vertical graphene sensor offers many new possibilities for sensors and is a feasible method for large-scale manufacturing of sensor devices.

To summarize, we report an FET VG sensor fabricated by direct growth of VG sheets on gold electrodes using a PECVD method. The vertical structure of VG facilitates the deposition of the Au NP-antibody conjugates on the sensor and the direct growth method improves the adhesion of the graphene sheet and the gold electrode, leading to enhanced sensor stability. The VG-based protein sensor shows a low detection limit, good specificity, and a short response time, which is excellent among graphene/CNT-based electronic sensors. Results from this study present a new method to design and fabricate graphene FET sensors and a promising route for the large scale manufacturing of sensor devices.

## Methods

**Materials.** Colloidal Au nanoparticles (10 nm) labeled with anti-IgG (anti-Human IgG (H + L)) and IgG from human serum were ordered from Tedpella and Sigma-Aldrich, respectively. The blocking buffer (BB) (SuperBlock T20 (PBS)) was ordered from Thermo Scientific. The PBS buffer solution (pH 7.4) was used as the IgG solvent (Fisher BioReagents). All reagents were used as received and the distilled and deionized water were ordered from Cellgro.

**VG sensor fabrication.** The VG sensor was fabricated by direct growth of VG sheets on the gold interdigitated electrodes (finger-width of several microns, inter-finger spacing of 2  $\mu\text{m}$ , and a thickness of 50 nm, similar to our previously used electrodes<sup>37</sup>) using a PECVD method; and experimental details of the VG growth can be found in our previously published paper<sup>39</sup>. In a typical procedure, Ar and CH<sub>4</sub> flows were introduced into the reactor (700 °C) with two separate flows: an Ar/CH<sub>4</sub> flow (10% CH<sub>4</sub> by volume, 1 lpm) and an Ar/water vapor flow (Ar flow through a bubbler flask, 0.1 lpm). The plasma reactor was designed with a tungsten pin cathode (3.5 kV) pointing toward the gold electrodes anode (grounded) with a distance of 1 cm. VG growth duration was 30 seconds for a sensor device and no catalyst was used throughout the VG growth.

**Structure characterization.** A Hitachi S-4800 UHR FE-SEM was used for scanning electron microscope characterization of the device at an acceleration voltage of 10 kV. A Hitachi H9000 NAR Transmission Electron Microscope was used for TEM, selected area diffraction (SAD), and EDX analyses.

**Sensor performance characterization.** For the sensing test, the VG sensor was first incubated with Au NP-anti-IgG conjugates for one hour and then incubated in a blocking buffer (BB) for two hours and thoroughly washed with a PBS buffer after incubation. The blocking buffer could efficiently block the non-specific protein bindings to VG sheets and electrodes; therefore, it was used to improve the sensor selectivity and reduce the uncertainty in the sensing signal. In a typical test, analyte protein (IgG, 1  $\mu\text{L}$ ) was pipetted onto the device for protein binding; after one hour, the sensor device was washed with DI water and dried. The sensor signal was recorded using a Keithley 2602 source meter for direct current and transistor measurements and a Keithley 4200 semiconductor characterization system for dynamic measurements. The direct current measurement was performed by recording the drain current with the drain-source voltage  $V_{ds}$  sweeping from  $-2.0$  to  $+2.0$  V with a

step of 0.1 V. In the transistor measurement, the drain current was measured with a fixed  $V_{ds}$  (0.1 V) while sweeping the gate voltage  $V_g$  from  $-40.0$  to  $+40.0$  V with a step of 0.1 V. The dynamic measurement was carried out by recording the drain current with a fixed  $V_{ds}$  throughout the sensing period. The sensing test was performed in an ambient environment at room temperature and the sensor repeatability was studied by using five sensors in each sensing test/condition.

- Geim, A. K. Graphene: Status and Prospects. *Science* **324**, 1530–1534 (2009).
- Geim, A. K. & Novoselov, K. S. The rise of graphene. *Nat. Mater.* **6**, 183–191 (2007).
- Guo, S. & Dong, S. Graphene nanosheet: synthesis, molecular engineering, thin film, hybrids, and energy and analytical applications. *Chem. Soc. Rev.* **40**, 2644–2672 (2011).
- Mao, S., Pu, H. & Chen, J. Graphene oxide and its reduction: modeling and experimental progress. *RSC Adv.* **2**, 2643–2662 (2012).
- Schedin, F. *et al.* Detection of individual gas molecules adsorbed on graphene. *Nat. Mater.* **6**, 652–655 (2007).
- Cohen-Karni, T., Qing, Q., Li, Q., Fang, Y. & Lieber, C. M. Graphene and Nanowire Transistors for Cellular Interfaces and Electrical Recording. *Nano Lett.* **10**, 1098–1102 (2010).
- He, Q. *et al.* Centimeter-Long and Large-Scale Micropatterns of Reduced Graphene Oxide Films: Fabrication and Sensing Applications. *ACS Nano* **4**, 3201–3208 (2010).
- Kuila, T. *et al.* Recent advances in graphene-based biosensors. *Biosens. Bioelectron.* **26**, 4637–4648 (2011).
- Mannoor, M. S. *et al.* Graphene-based wireless bacteria detection on tooth enamel. *Nat. Commun.* **3** (2012).
- Mao, S., Lu, G. H., Yu, K. H., Bo, Z. & Chen, J. H. Specific Protein Detection Using Thermally Reduced Graphene Oxide Sheet Decorated with Gold Nanoparticle-Antibody Conjugates. *Adv. Mat.* **22**, 3521–3526 (2010).
- Ohno, Y., Maehashi, K. & Matsumoto, K. Label-Free Biosensors Based on Aptamer-Modified Graphene Field-Effect Transistors. *J. Am. Chem. Soc.* **132**, 18012–18013 (2010).
- Yang, W. *et al.* Carbon Nanomaterials in Biosensors: Should You Use Nanotubes or Graphene? *Angew. Chem. Int. Ed.* **49**, 2114–2138 (2010).
- Zhang, Y. *et al.* One-pot green synthesis of Ag nanoparticles-graphene nanocomposites and their applications in SERS, H<sub>2</sub>O<sub>2</sub>, and glucose sensing. *RSC Adv.* **2**, 538–545 (2012).
- Chen, K. *et al.* Hg(II) Ion Detection Using Thermally Reduced Graphene Oxide Decorated with Functionalized Gold Nanoparticles. *Anal. Chem.* **84**, 4057–4062 (2012).
- Dong, Y. Q. *et al.* Graphene Quantum Dot as a Green and Facile Sensor for Free Chlorine in Drinking Water. *Anal. Chem.* **84**, 8378–8382 (2012).
- Fowler, J. D. *et al.* Practical Chemical Sensors from Chemically Derived Graphene. *ACS Nano* **3**, 301–306 (2009).
- Lu, G. *et al.* Toward Practical Gas Sensing with Highly Reduced Graphene Oxide: A New Signal Processing Method To Circumvent Run-to-Run and Device-to-Device Variations. *ACS Nano* **5**, 1154–1164 (2011).
- Mao, S. *et al.* Tuning gas-sensing properties of reduced graphene oxide using tin oxide nanocrystals. *J. Mater. Chem.* **22**, 11009–11013 (2012).
- Yavari, F. *et al.* High Sensitivity Gas Detection Using a Macroscopic Three-Dimensional Graphene Foam Network. *Sci. Rep.* **1** (2011).
- Dong, X. C., Shi, Y. M., Huang, W., Chen, P. & Li, L. J. Electrical detection of DNA hybridization with single-base specificity using transistors based on CVD-grown graphene sheets. *Adv. Mat.* **22**, 1–5 (2010).
- He, Q. *et al.* Transparent, Flexible, All-Reduced Graphene Oxide Thin Film Transistors. *ACS Nano* **5**, 5038–5044 (2011).
- Mohanty, N. & Berry, V. Graphene-based single-bacterium resolution biodevice and DNA transistor: interfacing graphene derivatives with nanoscale and microscale biocomponents. *Nano Lett.* **8**, 4469–4476 (2008).
- Park, S. J. *et al.* Ultrasensitive Flexible Graphene Based Field-Effect Transistor (FET)-Type Bioelectronic Nose. *Nano Lett.* **12**, 5082–5090 (2012).
- Xiao, F. *et al.* Coating Graphene Paper with 2D-Assembly of Electrocatalytic Nanoparticles: A Modular Approach toward High-Performance Flexible Electrodes. *ACS Nano* **6**, 100–110 (2012).
- Chuang, A. T. H., Robertson, J., Boskovic, B. O. & Koziol, K. K. Three-dimensional carbon nanowall structures. *Appl. Phys. Lett.* **90** (2007).
- Hiramatsu, M., Shiji, K., Amano, H. & Hori, M. Fabrication of vertically aligned carbon nanowalls using capacitively coupled plasma-enhanced chemical vapor deposition assisted by hydrogen radical injection. *Appl. Phys. Lett.* **84**, 4708–4710 (2004).
- Star, A., Gabriel, J. C. P., Bradley, K. & Gruner, G. Electronic detection of specific protein binding using nanotube FET devices. *Nano Lett.* **3**, 459–463 (2003).
- Tian, S. *et al.* Robust adhesion of flower-like few-layer graphene nanoclusters. *Sci. Rep.* **2** (2012).
- Wang, J. J. *et al.* Free-standing subnanometer graphite sheets. *Appl. Phys. Lett.* **85**, 1265–1267 (2004).
- Bo, Z. *et al.* Understanding growth of carbon nanowalls at atmospheric pressure using normal glow discharge plasma-enhanced chemical vapor deposition. *Carbon* **49**, 1849–1858 (2011).
- Yu, K., Lu, G., Bo, Z., Mao, S. & Chen, J. Carbon Nanotube with Chemically Bonded Graphene Leaves for Electronic and Optoelectronic Applications. *J. Phys. Chem. Lett.* **2**, 1556–1562 (2011).



32. Yu, K. *et al.* Patterning Vertically Oriented Graphene Sheets for Nanodevice Applications. *J. Phys. Chem. Lett.* **2**, 537–542 (2011).
33. Bai, S. & Shen, X. Graphene-inorganic nanocomposites. *RSC Adv.* **2**, 64–98 (2012).
34. Chen, R. J. *et al.* Noncovalent functionalization of carbon nanotubes for highly specific electronic biosensors. *Proc. Natl. Acad. Sci. USA* **100**, 4984–4989 (2003).
35. Chou, S. S. *et al.* Nanoscale Graphene Oxide (nGO) as Artificial Receptors: Implications for Biomolecular Interactions and Sensing. *J. Am. Chem. Soc.* **134**, 16725–16733 (2012).
36. Kwon, O. S. *et al.* Flexible FET-Type VEGF Aptasensor Based on Nitrogen-Doped Graphene Converted from Conducting Polymer. *ACS Nano* **6**, 1486–1493 (2012).
37. Mao, S., Yu, K., Lu, G. & Chen, J. Highly Sensitive Protein Sensor Based on Thermally-Reduced Graphene Oxide Field-Effect Transistor. *Nano Res.* **4**, 921–930 (2011).
38. Jung, I., Dikin, D. A., Piner, R. D. & Ruoff, R. S. Tunable electrical conductivity of individual graphene oxide sheets reduced at "low" temperatures. *Nano Lett.* **8**, 4283–4287 (2008).
39. Yu, K. *et al.* Growth of carbon nanowalls at atmospheric pressure for one-step gas sensor fabrication. *Nanoscale Res. Lett.* **6** (2011).

## Acknowledgments

Financial support for this work was provided by a U.S. NSF grant (IIP-1128158) and a University of Wisconsin-Milwaukee Research Foundation Bradley Catalyst Grant. The authors thank Dr. Heather A. Owen for technical support with SEM and Professor Marija

Gajdardziska-Josifovska for TEM access at the high-resolution TEM Laboratory at UWM. The e-beam lithography was performed at the Center for Nanoscale Materials of Argonne National Laboratory, which is supported by the U.S. Department of Energy (DE-AC02-06CH11357). The SEM imaging was conducted at the electron microscopy laboratory of UWM.

## Author contributions

S. M. and J. H. C. designed this research; K. H. Y. fabricated the VG sensor; L. O. fabricated the sensor electrode; S. M. carried out the sensor structure characterization and sensing test; J. B. C. and D. A. S. analyzed the data; S. M. and J. H. C. drafted the paper; and all authors commented on the final manuscript.

## Additional information

**Supplementary information** accompanies this paper at <http://www.nature.com/scientificreports>

**Competing financial interests:** The authors declare no competing financial interests.

**License:** This work is licensed under a Creative Commons Attribution-NonCommercial-NoDerivs 3.0 Unported License. To view a copy of this license, visit <http://creativecommons.org/licenses/by-nc-nd/3.0/>

**How to cite this article:** Mao, S. *et al.* Direct Growth of Vertically-oriented Graphene for Field-Effect Transistor Biosensor. *Sci. Rep.* **3**, 1696; DOI:10.1038/srep01696 (2013).